J. Plasma Physics (2011), *vol.* 77, *part* 2, *pp.* 277–287.
doi:10.1017/S0022377810000188

Single-species Weibel instability of radiationless plasma

L. V. BORODACHEV and D. O. KOLOMIETS

M.V. Lomonosov Moscow State University, Moscow 119991, Russia
(kolomiets@darwincode.org)

(Received 2 February 2010; revised 17 February 2010 and accepted 17 March 2010, first published online 16 April 2010)

Abstract. A particle-in-cell numerical simulation of the electron Weibel instability is applied in a frame of Darwin (radiationless) approximation of the self-consistent fields of sparse plasma. As a result, we were able to supplement the classical picture of the instability and, in particular, to obtain the dependency of the basic characteristics (the time of development and the maximum field energy) of the thermal anisotropy parameter, to trace the dynamic restructuring of current filaments accompanying the non-linear stage of the instability and to trace in detail the evolution of the initial anisotropy of the electron component of plasma.

1. Introduction

As it is well known, anisotropic distribution of thermal velocities in homogeneous collisionless plasma may lead to Weibel instability (WI) in case of spontaneous generation of transverse to direction of anisotropy magnetic field [1]. The peculiarity of WI is to have a regime where unstable growth of magnetic field generated by arisen current layers (filaments in multidimensional case) is followed by dynamic transformation of the current structures and stabilization of the magnetic field energy after saturation of the instability.

The general picture of WI mentioned above has significant variations in several of practically important applications of plasma physics, e.g. WI in relativistic plasma which absorbed high-energy electromagnetic impulse [2] is considerably different comparing to WI occurring in the current sheet of Earth's magnetotail [3], which in turn differs from WI of intense ion beams [4]. Recent researches indicate that WI might have an important role in dense quantum plasmas [5], where WI is supposed to be responsible for the generation of non-stationary magnetic fields in compact astrophysical objects as well as in laser fusion experiments.

That variety of forms along with fundamental nature of WI stimulate its further study using different approaches, one of which is a particle-in-cell method based on Vlasov–Darwin model [6] applied below. Presence of well-developed linear theory of electromagnetic instabilities [7], a typical representative of which is WI, allows one to verify the obtained numerical results.

This work is devoted to the numerical simulation of the electron WI in order to clarify its general picture, in particular, the evolution of the initial anisotropy on the time and the dependency of key instability characteristics of the initial anisotropy. Ions due to inertia are considered to be a neutralizing positive background.

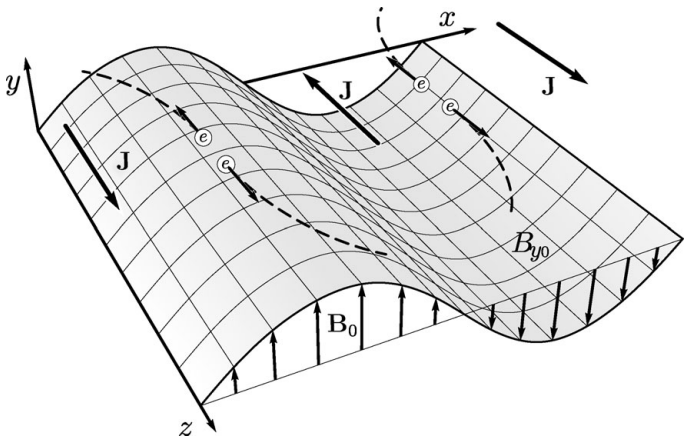

Figure 1. Qualitative representation of the linear phase of WI. Development of current sheets **J** around the zeros of B_y (shown as a surface). B_x, B_z considered zero for simplicity.

2. Elements of linear theory of Weibel instability

In order to get notion of the generation mechanism of the WI we will review the basic results of linear theory applied to it in the most simple, 1D3V (x, v_x, v_y, v_z), setup.

Let us consider a homogeneous collisionless plasma with a positive (ion) background and anisotropic distribution of thermal velocities of electrons, given by the following distribution function:

$$f_0(\mathbf{v}) = \frac{n_0 \exp\left(-\dfrac{v_x^2}{u_x^2} - \dfrac{v_y^2}{u_y^2} - \dfrac{v_z^2}{u_z^2}\right)}{\pi^{3/2} u_x u_y u_z}, \tag{2.1}$$

where n_0 is the density of electrons, u_x, u_y, u_z are the thermal velocities of the electrons along the corresponding axes, where we assume (without loss of generality) $u_z > u_x = u_y$.

In this case the plasma, obviously, has an excess of fast particles moving along z-axis. However, due to the symmetry of the distribution, the total current is zero.

Now assume that there exists spontaneously generated (due to thermal fluctuations) non-zero magnetic field $\mathbf{B}_0 = \mathbf{e}_y B_{y0} \sin(k_x x)$. Then the Lorentz force $\mathbf{F}_L = -e\mathbf{v} \times \mathbf{B}_0/c$ will change the trajectory of a particle moving along z, which will lead to formation of spatially separated current sheets. Localization of these sheets will coincide with the zeros of the magnetic field which caused the deflection of the particles. Hence, we should expect formation of two current sheets (with opposite signs) per each wavelength of the magnetic field perturbation, amplifying the initial magnetic field. The growth of the field, which in turn increases density of the current sheets, will continue until the major part of the particles become significantly magnetized. Figure 1 shows a qualitative illustration of this process.

In the described setup the perturbed quantities are $E_z(x,t)$, $B_y(x,t)$ (unperturbed values of which are zero) and the electron distribution function $f(x, \mathbf{v}, t) = f_0(\mathbf{v}) + f_1(x, \mathbf{v}, t)$.

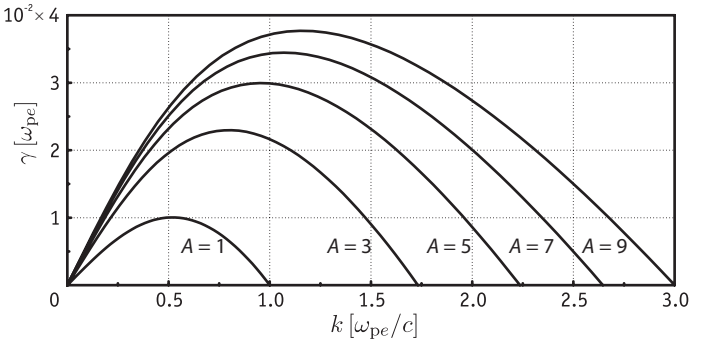

Figure 2. Growth rate of WI for various values of anisotropy at constant accentuated thermal velocity $u_z = 0.1\ [c]$.

Let the perturbations (as it is common for linear analysis in general) to be represented as $\exp(i(k_x x - \omega t))$. Then, substituting the corresponding values into the Vlasov equation and the field equations, we obtain (as it is shown in [8]) a dispersion equation

$$k_x^2 c^2 - \omega^2 = \omega_{pe}^2 \left(A + \frac{\omega\,(A+1)}{k_x u_x} Z\left(\frac{\omega}{k_x u_x}\right)\right), \tag{2.2}$$

where $\omega_{pe} = \sqrt{4\pi n_0 e^2/m}$ is the electron plasma frequency, $A = (u_z^2/u_x^2 - 1)$ is the anisotropy parameter and Z is the plasma dispersion function [9]:

$$Z\,(\zeta) = \frac{1}{\sqrt{\pi}} \int_{-\infty}^{\infty} \frac{e^{-s^2}}{s-\zeta}\, ds, \tag{2.3}$$

where ζ in general is a complex value.

The unstable roots of (2.2) (solutions with purely imaginary positive ω, the standing waves) are in the range from $kc/\omega_{pe} = 0$ to $kc/\omega_{pe} = \sqrt{A}$ for any $A > 0$. Thus, in the case when the dimensionless wave number k_x falls into that interval, there is a sharp increase in the amplitude of the perturbation of the corresponding wavelength, which is a key feature of the initial stage of WI. The growth rate $\gamma = i\omega$ has a single maximum in the above-mentioned range, which allows to determine the most unstable mode. Note that it is hard (if at all possible) to get analytical solution of this equation, but it is rather easy to solve it numerically with any standard method [10]. The foregoing is illustrated in Fig. 2 where the graphs of the growth rate are shown for various values of anisotropy parameter with fixed accentuated thermal velocity u_z.

3. Numerical simulations

Here we will briefly review the basic features of the model we chose, as well as its geometrical setup and the main parameters.

The general physical properties of the system were already described above in the Sec. 2. Now we will consider 2.5-dimensional setup (x, y, v_x, v_y, v_z), where the accentuated component of the thermal velocity is taken perpendicularly to the simulation plane x–y. Note that in this case the development of the instability will

now be supported with formation of current filaments (beams), rather than layers, as it was in 1.5 dimensions. However, the results of the linear theory presented above are still valid in this case, if one assumes $k_x = k_y = k$.

First of all, we should note that low-frequency nature of the WI itself allows us to use Darwin (radiationless) approximation of the electromagnetic fields [11], which is significantly more efficient from computational point of view comparing to more common full Maxwell model.

Thus, in the particle-in-cell simulations performed here, the evolution of plasma system inside of the computational domain described by the dynamic equations of macroparticles (electrons)

$$\begin{cases} \dfrac{d\mathbf{v}_p}{dt} = \dfrac{q_p}{m_p}\left(\mathbf{E}(\mathbf{r}_p, t) + \dfrac{\mathbf{v}_p \times \mathbf{B}(\mathbf{r}_p, t)}{c}\right), \\ \dfrac{d\mathbf{r}_p}{dt} = \mathbf{v}_p, \quad p = 1, 2, \ldots, N_\mathrm{p}, \end{cases} \tag{3.1}$$

moving in the self-consistent fields determined by the Darwin's equations

$$\begin{cases} \nabla \times \mathbf{B} = \dfrac{4\pi}{c}\mathbf{J} + \dfrac{1}{c}\dfrac{\partial \mathbf{E}_l}{\partial t}, \\ \nabla \mathbf{B} = 0, \\ \nabla \times \mathbf{E}_t = -\dfrac{1}{c}\dfrac{\partial \mathbf{B}}{\partial t}, \\ \nabla \mathbf{E}_l = 4\pi\rho, \\ \mathbf{E} = \mathbf{E}_l + \mathbf{E}_t, \quad \nabla \times \mathbf{E}_l = 0, \quad \nabla \mathbf{E}_t = 0, \end{cases} \tag{3.2}$$

where $\mathbf{E}_l$ and $\mathbf{E}_t$ are, correspondingly, the longitudinal (curl-free) and transverse (divergence-free) components of the electric field.

As it is easy to see, Darwin's approximation differs from the full Maxwell description only by the eliminated transverse displacement current, which physically means neglecting radiation and transition to fields with instantaneous propagation [12]. At the same time the system partially keeps inductive effects (associated with Faraday's law) and ensures holding of the continuity equation due to the presence of longitudinal part of the displacement current.

Next, we specify the uniform spatial distribution of electrons and singly charged ions, the latter ones are considered as a motionless neutralizing background. In the expression (2.1) we choose $u_z = 0.1\,[c]$, $u_x = u_y = 0.0316\,[c]$. For these values of thermal velocities the anisotropy parameter equals to $A_0 = 9$.

The characteristic linear size of the computational domain, which we can choose for the simulation, must correspond to the wavelength for which the dispersion equation (for given values of anisotropy and accentuated thermal velocity) shows the instability growth rate close to maximum (Fig. 2).

In particular, solving numerically (2.2) for our reference case $A_0 = 9$ and $u_z = 0.1\,[c]$, we obtain the approximate value of $\gamma_{\max} = 0.037$ and the corresponding value of $k_{\max} = 1.2\,[\omega_{\mathrm{p}e}/c]$, in terms of the wavelength it will give us $\lambda_{\max} = 5.2\,[c/\omega_{\mathrm{p}e}]$.

Thus, choosing a rectangular computational domain $L_x = L_y = 25\,[c/\omega_{\mathrm{p}e}]$ will allow us to trace in detail the development of initial current system and its restructuring in non-linear stage of WI.

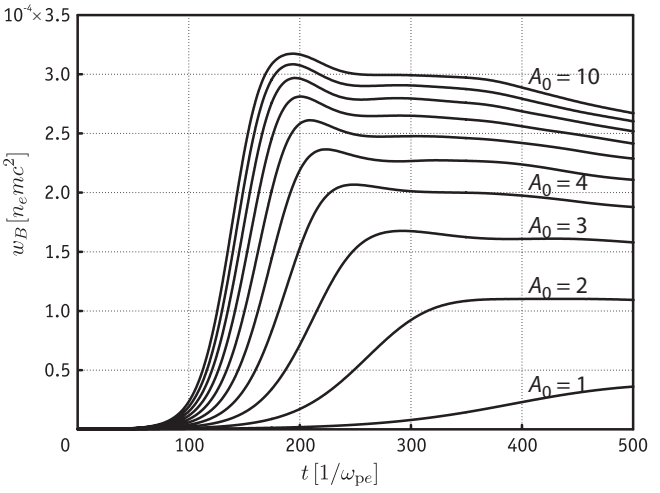

Figure 3. Average magnetic field energy density versus time for different values of initial anisotropy ($A_0 = 1 \ldots 10$) at constant accentuated thermal velocity. Computational domain $L_x = L_y = 25\,[c/\omega_{pe}]$; $u_z = 0.1\,[c]$; mesh size 128×128; 500 particles of each specie per cell; time step $\tau = 0.25\,[1/\omega_{pe}]$.

Determination of the total number of particles N_p is preconditioned by a natural trade-off between holding collisionless property of the model in the time-frame sufficient for development of the instability and computational cost of a single run. Using theoretical estimations of the collisionless time for big particles (with width $W > \lambda_D$) [13], as well as test runs, it was found that the number of particles N_p of order 10^6 allows to have the collisionless period at least five times longer than it is needed for the development of WI.

Following the work [8], we choose periodic boundary conditions for both x and y directions.

Finally, note that in the series of experiments considered below variation of the the initial anisotropy parameter A_0 has been done by changing of u_x and u_y keeping u_z constant in all runs to keep non-relativistic regime of the simulations.

4. Discussion of results

The instability development process is clearly visible on the plots of the average over space magnetic field energy density versus time for different initial values of the anisotropy shown in Fig. 3. The initial value of the average energy density is close to zero, but by the time $t = 100\,[1/\omega_{pe}]$, corresponding to appearing of distinguishable areas of current localization, it is observed a noticeable increase, which is the greater the larger is the initial anisotropy of the plasma. As noted above, the linear stage ends when the system formed a pronounced current structure consisting of a system of current beams (Fig. 6, time slice $t = 150\,[1/\omega_{pe}]$), and when the particles become significantly magnetized in average (mean Larmor radius is of the order of the current beam radius).

Further development of the WI is non-linear and is accompanied by dynamic merging of equidirected current filaments into larger-scale structures, which can be

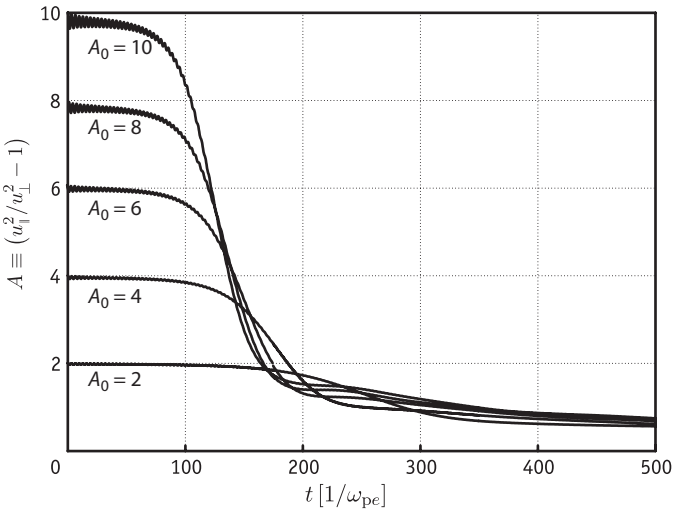

Figure 4. Evolution of the anisotropy for different initial A_0. The same numerical setup as for Fig. 3.

seen from a series of time slices shown in Fig. 6. Along with that the magnitude of the magnetic field energy stabilizes. Here we would note that this picture is quite similar to one considered in [14], where the authors study filament recombination which take place on the non-linear stage of WI arising with propagation of relativistic electron beam in background plasma (a theory of relativistic coalescence has been developed in [15, 16]).

The merging continues until the velocity distribution of the electrons does not become an equilibrium. In that context it is interesting to trace the evolution of the initial anisotropy of the electron component during the development of WI, including at the non-linear stage. The dependency of the anisotropy on the time is shown in Fig. 4. From the figure one can see that the process of growth and further stabilization of current density and magnetic field energy density is accompanied by isotropization (decrease in the anisotropy) of the medium, caused by collective processes of formation and restructuring of current filaments together with competitive development of the unstable modes of the magnetic field.

It is interesting to note here an non-obvious fact that regardless of the initial value of the the anisotropy, its value at the instability saturation stage tends to a non-zero threshold value (see Fig. 4).

The origin for that residual anisotropy is in the problem setup, and it is connected with an actual finiteness of the perturbation spectrum of any system with periodic boundary conditions due to the fact that in such a system waves longer than linear size of the domain cannot exist.

This conclusion is confirmed by the results of [17], where it is shown that for a limited system (in the sense stated above) the minimum level of the anisotropy at the saturation stage of WI can be defined by the following expression:

$$A_{\min} = (k_{\min} c/\omega_{pe})^2. \tag{4.1}$$

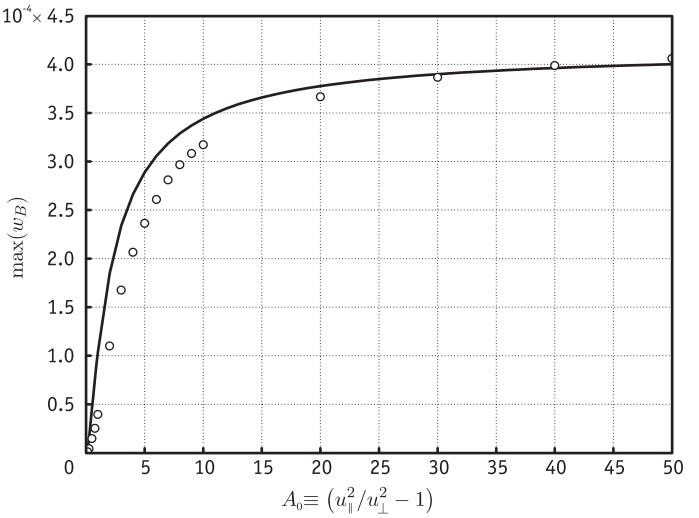

Figure 5. The dependency of the maximum average magnetic field energy density of the initial anisotropy at constant accentuated thermal velocity $u_z = 0.1\,[c]$. The same setup as for Fig. 3.

In our case the minimal wave number allowed in the system is $k_{\min}c/\omega_{pe} = 0.25$, which gives $A_{\min} = 0.063$. Some discrepancy of the experimentally observed levels of residual anisotropy (Fig. 4) and its theoretically predicted value can be explained by the fact, that at time $t = 500\,[1/\omega_{pe}]$ the dominant mode of the instability has not yet reached the limit determined by the period of the system. As stated above, one of the objectives of these experiments was to clarify the dependency of the basic characteristics of the instability – its growth rate, the characteristic time and the maximum energy density of the magnetic field, of the initial anisotropy of plasma.

In this connection let us return to Fig. 3, from which one can see the expected effect: the increase of the maximum field energy density and instability growth rate with the increase of initial anisotropy. Less trivial is the profile of this dependency shown in Fig. 5: fast increase of the maximum energy density on the interval $A_0 < 10$, followed by an equally fast drop-off with $A_0 > 10$.

Moreover the value of A_0 around 25 can be considered as an upper threshold of instability in the sense that further increase in the initial anisotropy of electron component has virtually no effect on the basic characteristics of the WI – the maximum value of magnetic field energy density (in case of fixed value of accentuated thermal velocity u_z). The observed effect and its quantitative characteristics are confirmed by analytical expression which can be obtained on the basis of the expression derived in the work [17]:

$$\frac{w_B}{n_0 T_{z0}} = \frac{1}{3}\left(\frac{A}{A+1}\right)\left(\frac{1}{A+1} - \frac{1}{A_0+1}\right), \tag{4.2}$$

where T_z is the temperature of accentuated electron component along z-axis.

In the just mentioned work the expression (4.2) has been used as an estimation of evolution of the magnetic field energy density, where the values of A were being taken from the numerical simulation.

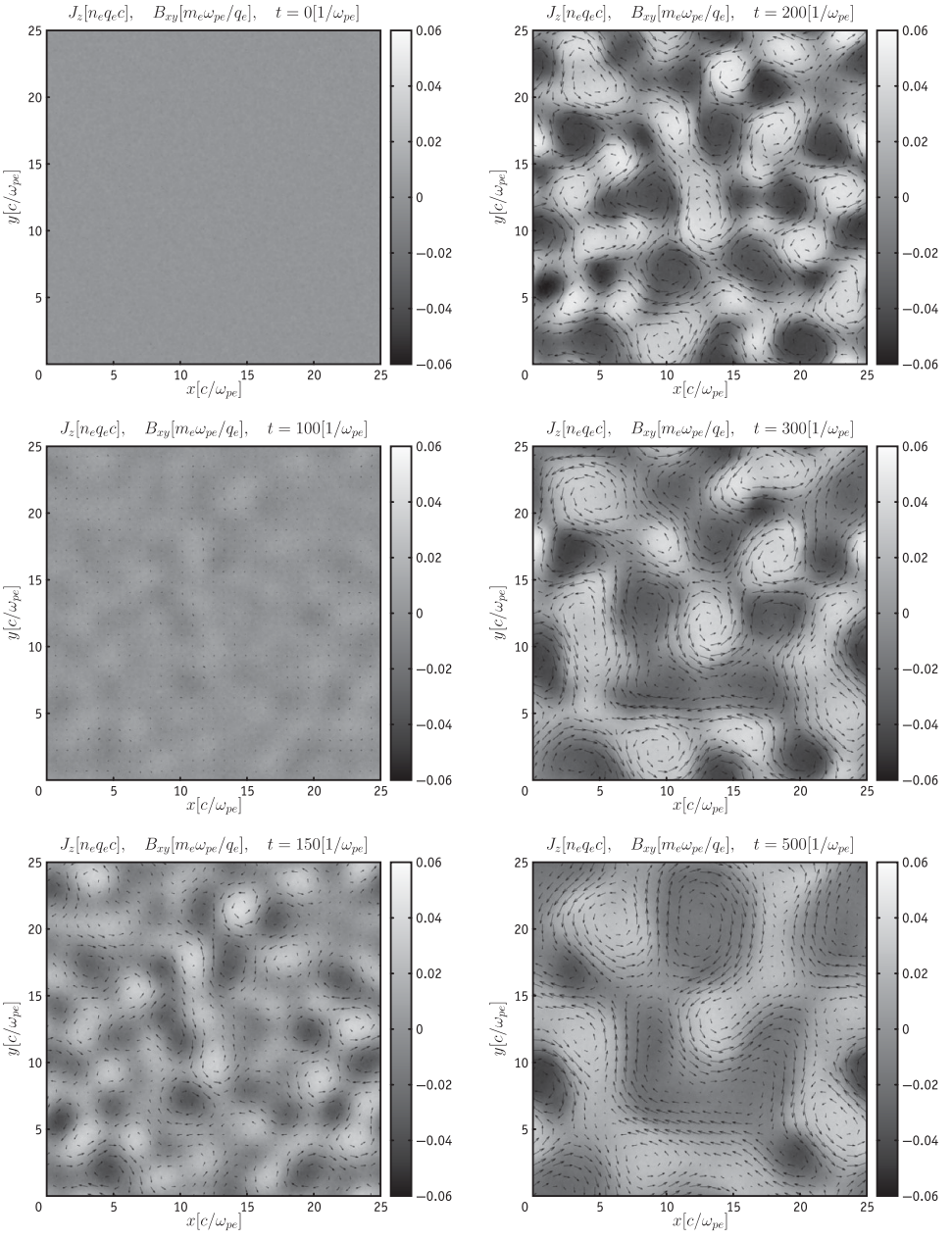

Figure 6. The current density J_z and the magnetic field $\mathbf{B}_{xy}$ at different time moments for 2.5-dimensional setup of WI in case $A_0 = 9$. Computational domain $L_x = L_y = 25\,[c/\omega_{pe}]$; $u_z = 0.1\,[c]$; mesh size 256×256; 1000 particles of each specie per cell; time step $\tau = 0.25\,[1/\omega_{pe}]$.

However, in our context, it can be interpreted as an analytical dependency of the magnetic field energy density (in units of $n_0 T_z$) of the current value of anisotropy A with its initial value given as A_0. Considering (4.2) that way, its easy to get

an interesting for us estimation of the maximum energy of WI (or, equivalently, the maximum proportion of the energy of accentuated component which can be converted into field energy) and also the explanation of the existence of upper threshold of WI on A_0 mentioned above. Indeed, differentiating the right-hand side of (4.2) with respect to A and equating the derivative to zero we obtain

$$\frac{A_0 - A(2 + A_0)}{3(A + 1)^2(A_0 + 1)} = 0. \tag{4.3}$$

Where from we get the value of the anisotropy coefficient which delivers the maximum to the expression (4.2) with fixed value of A_0:

$$A_{\text{extr}} = \frac{A_0}{2 + A_0}. \tag{4.4}$$

Substituting the resulting value of A_{extr} back into (4.2), we find the desired dependence of the maximum magnetic field energy on the value of A_0:

$$w_{B\max} = \frac{n_0 T_{z0} A_0^2}{12(1 + A_0)^2}. \tag{4.5}$$

Dependency (4.5) together with the experimental values is shown in Fig. 5.

Analysis of the last expression gives a number of interesting provisions which are in good agreement with computer simulation experiments.

First, $w_{B\max}$ has a limit in case of fixed values of n_0, T_{z0} (u_z) and $A_0 \to \infty$ (the last one actually means $u_x, u_y \to 0$):

$$w_{B\max}^{\lim} = \frac{n_0 T_{z0}}{12}, \tag{4.6}$$

corresponding to the maximum possible energy density of WI. Particularly, in our case, where $n_0 T_{z0} = 0.005\,[n_e mc^2]$, $w_{B\max}^{\lim}$ equals to $4.1 \cdot 10^{-4}\,[n_e mc^2]$, which, as it can be seen in Fig. 5, is in good agreement with the numerical data.

Second, observed in experiments, the upper threshold of WI with respect to A_0 is determined by the value of A_0, starting from which the fraction $A_0^2/(1 + A_0)^2$ becomes close to unity. It is easy to see that the value of A_0 close to 25 meets this requirement (indeed, if $A_0 = 25$ the fraction equals to 0.925, and if $A_0 = 50$, i.e. increased by factor of two, it only slightly increases up to 0.96).

Third, the portion of energy stored in the accentuated component of the system which goes for development of WI depends on the degree of the initial anisotropy (A_0) and it cannot be higher than 1/12. For instance, in our experiments it varies from 6.2% (for $A_0 = 9$) down to 2.2% (for $A_0 = 2$). These data are consistent both with the analytical predictions obtained from the expression (4.5) and with the upper limit of the converted anisotropy energy (around 10%) obtained in [8], where two-dimensional simulation has been performed in the frame of full electromagnetic model of plasma.

If we define the characteristic time of the instability (T_I) as the time needed to reach the maximum of magnetic field energy density, then from the same Fig. 3 one can easily estimate both the value of T_I as well as it's dependence of the initial anisotropy A_0.

Finally, we note good agreement between the numerical value of the dimensionless instability growth rate (0.034) with the one predicted by the linear theory (0.037) for the setup considered above where $A_0 = 9$ and $u_z = 0.1\,[c]$.

5. Conclusions

Thus, the performed computer experiments allowed to supplement the classical picture of the WI. Particularly, we obtained the dependency of the characteristic time of its development and the maximum magnetic field energy density of the initial value of the anisotropy parameter. Also we have traced the dynamic restructuring of the current filaments accompanying non-linear stage of instability saturation, as well as the evolution of the initial anisotropy of the electron component of the plasma.

As a further work it is planned to perform a numerical study of the dynamics and generation mechanisms of two-species WI, which implies a kinetic representation not only of the electron but also the ion plasma component on the time scale by orders of magnitude grater than it is for a single-species WI.

Simulations have been performed on SKIF MSU 'Chebyshev' cluster of Moscow State University Research Computing Center.

Acknowledgements

The authors consider it their pleasant duty to thank Acad. L. M. Zelenyi and Dr. H. V. Malova from Russian Space Research Institute for numerous constructive discussions of the results presented in this work.

References

[1] Weibel, E. S. 1959 Spontaneously growing transverse waves in a plasma due to an anisotropic velocity distribution. *Phys. Rev. Lett.* **2**, 83–84.

[2] Pukhov, A. and Meyer-ter-Vehn, J. 1996 Relativistic magnetic self-channeling of light in near-critical plasma: three-dimensional particle-in-cell simulation. *Phys. Rev. Lett.* **76**(21), 3975–3978.

[3] Yoon, P. H. and Lui, A. T. Y. 1996 Nonlocal ion-Weibel instability in the geomagnetic tail. *J. Geophys. Res.* **101**(A3), 4899–4906.

[4] Davidson, R. C., Startsev, E. A., Kaganovich, I. and Qin, H. 2005 Multispecies Weibel instability for intense ion beam propagation through background plasma. In: *Proceedings of PAC*, pp. 1952–1954.

[5] Tsintsadze, L. N. and Shukla, P. K. 2008 Weibel instabilities in dense quantum plasmas. *J. Plasma Phys.* **74**(4), 431–436.

[6] Borodachev, L. V., Mingalev, I. V. and Mingalev, O. V. 2008 Vlasov–darwin system. In *Encyclopedia of Low Temperature Plasma (Series B)*, **VII**, pp. 136–146. Janus-K.

[7] Mikhailovsky, A. B. 1975 *Theory of Plasma Instabilities*. Atom Press.

[8] Morse, R. L. and Nielson, C. W. 1971 Numerical simulation of the Weibel instability in one and two dimensions. *Phys. Fluids*, **14**(11), 830–840.

[9] Frank-Kamenetskii, D. A. 1964 *Lectures on Plasma Physics*. Atom Press.

[10] Kalitkin, N. N. 1978 *Numerical Methods*. Nauka.

[11] Darwin, C. G. 1920 Dynamical motions of charged particles. *Phil. Mag.* **39**, 537–546.

[12] Nielson, C. W. and Lewis, H. R. 1976 Particle-code methods in the nonradiative limit. *Methods Comput. Phys.* **16**, 367–388.

[13] Hockney, R. W. and Eastwood, J. W. 1988 *Computer Simulation Using Particles*. CRC Press.

[14] Lee, R. and Lampe, M. 1973 Electromagnetic instabilities, filamentation, and focusing of relativistic electron beams. *Phys. Rev. Lett.* v. **31**(23), 1390–1393.

[15] Medvedev, M. V., Fiore, M., Fonseca, R. A., Silva, L. O. and Mori, W. B. 2005 Long-time evolution of magnetic fields in relativistic gamma-ray burst shocks. *Astrophys. J.* v. **618**, L75–L78.

[16] Polomarov, O., Kaganovich, I. and Shvets, G. 2008 Merging of super-Alfvénic current filaments during collisionless Weibel instability of relativistic electron beams. *Phys. Rev. Lett.* v. **101**, 175001.

[17] Lemons, D. S., Winske, D. and Gary, S. P. 1979 Nonlinear theory of the Weibel instability. *J. Plasma Phys.* **21**(2), 287–300.